5-2013

# Improving The Catalytic Activity Of Semiconductor Nanocrystals Through Selective Domain Etching

Elena Khon

Kelly Lambright

Rony S. Khnayzer

Pavel Moroz

Dimuthu Perera

*See next page for additional authors*

NANO LETTERS

Letter

pubs.acs.org/NanoLett

# Improving the Catalytic Activity of Semiconductor Nanocrystals through Selective Domain Etching

Elena Khon,[†,§] Kelly Lambright,[‡] Rony S. Khnayzer,[†,‡] Pavel Moroz,[†,§] Dimuthu Perera,[§] Evgeniia Butaeva,[†,‡] Scott Lambright,[§] Felix N. Castellano,[†,‡] and Mikhail Zamkov*[,†,§]

[†]The Center for Photochemical Sciences, [‡]Department of Chemistry, and [§]Department of Physics, Bowling Green State University, Bowling Green, Ohio 43403, United States

Supporting Information

**ABSTRACT:** Colloidal chemistry offers an assortment of synthetic tools for tuning the shape of semiconductor nanocrystals. While many nanocrystal architectures can be obtained directly via colloidal growth, other nanoparticle morphologies require alternative processing strategies. Here, we show that chemical etching of colloidal nanoparticles can facilitate the realization of nanocrystal shapes that are topologically inaccessible by hot-injection techniques alone. The present methodology is demonstrated by synthesizing a two-component CdSe/CdS nanoparticle dimer, constructed in a way that both CdSe and CdS semiconductor domains are exposed to the external environment. This structural morphology is highly desirable for catalytic applications as it enables both reductive and oxidative reactions to occur simultaneously on dissimilar nanoparticle surfaces. Hydrogen production tests confirmed the improved catalytic activity of CdSe/CdS dimers, which was enhanced 3−4 times upon etching treatment. We expect that the demonstrated application of etching to shaping of colloidal heteronanocrystals can become a common methodology in the synthesis of charge-separating nanocrystals, leading to advanced nanoparticles architectures for applications in areas of photocatalysis, photovoltaics, and light detection.

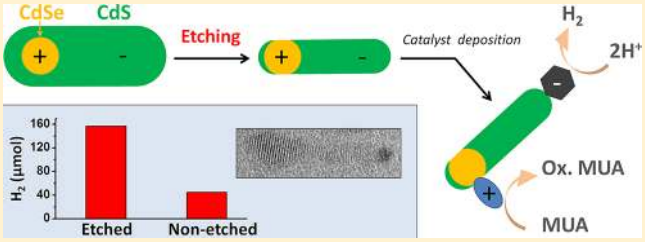


**KEYWORDS:** *Photovoltaics, catalysis, nanocrystals, etching, titanium dioxide*

Colloidal semiconductor nanocrystals (NCs) are emerging as promising building blocks for next-generation optoelectronic materials deployable in many device technologies including, solar cells,[1] lasers,[2] biomedical labels,[3] photoanodes,[4] and light-emitting diodes.[5] Our ability to incorporate application-specific combinations of properties within these nanostructures often depends on the existence of synthetic protocols for conjoining two or more dissimilar domains into a single heteronanocrystal. Many of these composite architectures can be obtained by means of standard colloidal techniques, in which one semiconductor component is used as a nanoparticle seed for nucleating the growth of the secondary domain.[6−8] This approach can lead to a variety of heteronanocrystal morphologies ranging from spherical core/shell,[9] to one-dimensional dot-in-a-rod,[10] tetrapod,[11] or barbell[12] structures.

Some shapes of heteronanocrystals, however, cannot be obtained by means of colloidal hot-injection techniques alone. An important class of composite nanocrystals that requires going beyond conventional colloidal growth is represented by a two-component structure, assembled in such a way that both semiconductor surfaces are exposed to the external environment. This type of the nanoparticle morphology is of considerable interest for catalytic applications, as it allows for different surfaces of the same heteronanocrystal to exhibit different chemical reactivity. In particular, a pair of semiconductors can be chosen to promote a greater electron density on one side of the composite nanoparticle while forcing the other domain to become hole-rich. Consequently, both semiconductor components in these nanoparticles can share the absorbed energy with external environment directly through the ligand-mediated charge transfer or via a metal catalyst (Figure 1a). Unfortunately, such domain topology cannot be easily achieved using a traditional seeded-growth approach, wherein one of the semiconductor components is fully surrounded by the secondary material, diminishing an overall catalytic activity of the nanoparticle. One previously considered solution that permits colloidal hot-injection route to yield two-component heteronanocrystals with exposed surfaces relies on coupling two semiconductors with strongly mismatched lattices.[13−15] This results in the formation of a structure where the semiconductor deposited in the second step forms island-like features on the surface of the "seed" component. This strategy, however, is hampered by the fact that in most relevant semiconductor heterostructures (e.g., CdSe/CdS, CdSe/CdTe, ZnSe/CdS) the interdomain lattice stress in insufficient to result in the fragmentation of the shell

**Received:** January 11, 2013
**Revised:** March 20, 2013
**Published:** March 29, 2013

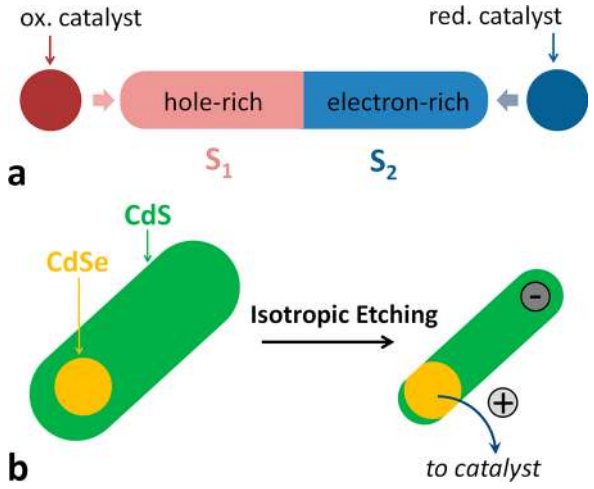


**Figure 1.** (a) Schematic representation of a catalytically active semiconductor heteronanocrystal. Ideally, both electron- and hole-rich semiconductor domains should be exposed to the surface in order to promote enhanced reactivity or to allow for catalyst deposition. (b) Illustration of the etching-based approach to the synthesis of two-component heteronanocrystals shown in (a). By etching an outer layer of CdS in a CdSe/CdS dot-in-a-rod structure, it is possible to obtain the morphology where both donor and acceptor components are in direct contact with the external environment.

component, causing only one type of material to be present on the surface of the heteronanocrystal.

Etching of colloidally grown nanocrystals provides a versatile tool for shaping the structure of incorporated domains. This method has been explored previously for tuning the morphology of metal nanoparticles, such as Au nanorods[16−19] and Ag-tipped Au barbells[20] toward enhancing their catalytic activity. On the other hand, application of etching techniques to semiconductor nanocrystals has received less attention and so far has been limited to several examples of tuning the size of binary nanocrystals. For instance, etching-mediated blue-shifting of the fluorescence emission has been reported for several semiconductor nanostructures, including CdS,[21,22] PbS,[23] CdSe,[24−26] CdTe,[27,28] and InP[29] NCs. In these reports, the etching mechanism relied on chemical or photooxidative dissolution of surface atoms. Anisotropic etching was also reported for semiconductor nanorods and tetrapods where chemical and photochemical techniques were combined together to provide facet selectivity.[30] Despite an apparent potential of the etching-based methods in nanoparticle synthesis, to date there have been no studies on etching of composite semiconductor NCs. In the meantime, the greatest capacity of the etching approach is anticipated from the application of this technique to multidomain nanocrystals, where it can result in novel topologies that are unattainable by conventional colloidal methods.

Here, we demonstrate that chemical etching of semiconductor nanocrystals represents a powerful tool for synthesizing novel structural morphologies, which give rise to enhanced catalytic activity of nanoparticle colloids. The method is exemplified by performing isotropic etching of colloidal nanostructures consisting of two spatially asymmetric material domains. This results in the formation of dimerlike structures where both donor and acceptor components are in direct contact with external environment. The open-surface arrangement of two materials leads to a substantial enhancement in the rate of oxidative and reductive processes occurring on heteronanocrystal surfaces. In particular, we show that chemical etching of CdSe/CdS dot-in-a-rod structures promotes a partial dissolution of the CdS shell from the surface of CdSe dots, which allows for a CdSe domain to come into a direct contact with the surrounding medium (Figure 1b). Such nanoparticle geometry facilitates the transfer of photoinduced holes away from the CdSe domain thus completing the proton reduction cycle initiated on the electron-rich CdS side. An improved catalytic performance of etched heteronanocrystals was confirmed in multiple tests through the observation of a 3−4 fold increase in the rate of hydrogen production by Pt-tipped CdSe/CdS dimers. The increased $H_2$ yield was attributed to an enhanced rate of hole regeneration in etched heteronanocrystals, which prevents backward recombination of dissociated excitons. This hypothesis was subsequently verified by time-resolved fluorescence (FL) measurements indicating that etching of a 0.7 nm CdS layer from CdSe/CdS nanorods decreased the CdSe-to-ligand hole transfer time from 3.7 to 1.3 ns. On a more global note, we expect that the preferred type of heteronanocrystal architecture for utilization in homogeneous catalysis will, ultimately, be the one that contains clearly segregated donor and acceptor components. In this sense, etching seems to be the most natural and potentially the easiest way for obtaining such nanoparticle geometries. We expect that any heteronanocrystal with even a slight nonsymmetric placing of the two domains can be etched to yield clearly segregated electron and hole domains.

While the present study is focused primarily on the catalytic performance of etched nanoparticles, the application of etching techniques to enhancing specific properties of colloidal heteronanocrystals is expected to find widespread utilization in many other nanocrystal technologies, including solar energy production and light detection. Indeed, both of these applications require spatial separation of photoinduced charges by the nanocrystal, which is best achieved when both donor and acceptor domains are exposed to the external environment. As this study demonstrates, an open-surface domain configuration leads to an improved transfer of photoinduced charges from nanocrystals to external moieties such as a solvent, a conjugated bridge, or an electrode.

CdSe/CdS dot-in-a-rod heteronanocrystals[10] were chosen as a suitable model system for studying the dynamics of etching in two-domain structures. First, the nonspherical arrangement of CdSe and CdS components within the nanoparticle allows exposing both semiconductor domains simply by removing an outer layer of the CdS material (Figure 1b). This can be achieved in a straightforward manner, by using isotropic etching techniques that rely on chemical dissolution of surface atoms. Second, when the size of the CdSe dot is sufficiently small, the hole becomes pinned by the potential barrier at the CdSe/CdS interface, which promotes photoinduced charge separation,[31] and third, catalyst-decorated dot-in-a-rod heteronanocrystals comprising such material combinations as CdSe/CdS,[32] ZnSe/CdS,[33] or all-CdS[7,34−36] are known to efficiently generate $H_2$ under visible illumination with quantum yields as high as 15%.[37] It is expected that a competitive catalytic performance of these nanostructures along with the high extinction coefficient in the visible and the ease of catalyst/product separation will make CdSe/CdS/Pt heterostructures promising catalytic materials for solar driven redox reactions.

The synthesis of CdSe/CdS heteronanocrystals for etching experiments was performed according to the previously


dx.doi.org/10.1021/nl400715n | Nano Lett. 2013, 13, 2016−2023

reported methodology,[10] as described in the Supporting Information section. In brief, small-diameter CdSe NCs ($\lambda_{band\text{-}edge}$ < 540 nm), prepared using hot-injection routes were used as nanoparticle seeds for nucleating the growth of CdS domains. The length and the width of CdSe/CdS dot-in-a-rod structures were controlled by tuning the amount and the diameter of CdSe nanocrystal seeds, respectively. To ensure a quasi-type II localization of carriers across CdSe/CdS nanorods corresponding to a partial confinement of a photoinduced hole within the CdSe dot portion, the size of CdSe NC seeds was kept below 3.0 nm (except in structural characterization tests where large diameter CdSe were intentionally used for imaging purposes).[31] A characteristic image of CdSe/CdS nanorods grown under aforementioned synthetic conditions is shown in Supporting Information Figure SF1.

Controlled etching of heteronanocrystals was achieved by introducing a mild solution of benzoyl peroxide (BPO) into solvent-dispersed NCs.[38,39] Prior to BPO treatment, the original ligands on the surface of CdSe/CdS nanoparticles were exchanged to a shorter benzylamine. This step allowed improving the reproducibility of the etching procedure, as benzylamine molecules partly replace facet-selective *n*-hexylphosphonic acid (HPA) and tri-*n*-octylphosphine (TOP) ligands that may potentially promote different etching rates. The effect of BPO treatment on optical spectra of CdSe/CdS heteronanocrystals is illustrated in Figure 2a. During a dropwise

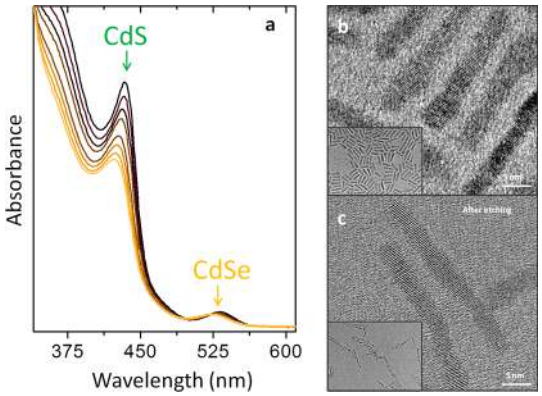


**Figure 2.** (a) Changes in the absorbance of CdSe/CdS nanorods caused by BPO treatment. Disappearance of the excitonic features ($\lambda$ = 450 nm for CdS and $\lambda$ = 530 nm for CdSe domains) reflects the etching-induced reduction of the nanocrystal volume. (b) A TEM image of CdSe/CdS nanorods before etching. A low-magnification TEM image of the same nanorods sample is shown in the insert. (c) A TEM image of CdSe/CdS nanorods after etching. The insert in (c) shows excessively etched nanorods, corresponding to the absorbance change in Supporting Information Figure SF2.

injection of BPO solution into the NC sample, $1S(e)1S_{3/2}(h)$ excitonic transitions associated with CdS ($\lambda$ = 450 nm) and CdSe ($\lambda$ = 530 nm) domains of nanorods underwent a noticeable blue shift, which was accompanied by the simultaneous broadening of the absorption edge. This trend was further continued upon additional injections of BPO until exciton absorption features of both CdS and CdSe components became indistinguishable (shown in Supporting Information Figure SF2). Transmission electron microscopy (TEM) spectra of etched (Figure 2c) and excessively etched (Figure 2c, insert) NCs confirm that the observed changes in the absorbance spectra were caused primarily by the reduction in the nanorod diameter. The corresponding changes in the emission of these structures are illustrated in Supporting Information Figure SF8.

The application of the etching treatment was optimized to yield dimerlike structures, whereby the shape of the original CdSe domain was mostly preserved while the dissolution of the CdS semiconductor on its surface was maximized. To this end, the addition of BPO was typically discontinued when the exciton absorbance edge of the CdSe component blue shifted by no greater than 10 nm. At this point, the band edge absorption of the CdS domain was reduced by about 50−70% indicating that a significant portion of CdS material was removed. TEM images of CdSe/CdS nanocrystals before and after etching confirm the reduction of the CdS phase (Figure 2b).

Figure 3a shows a representative TEM image of a single, BPO-treated CdSe/CdS nanorod comprising a large diameter CdSe seed ($d$ = 4.1 nm, see Supporting Information Figure SF3). By employing large CdSe NCs, it was possible to "tag" the location of the seed in grown nanorod structures (see also Figure 3b and Figure 5). The investigated specimen shows a considerable variation of the CdS diameter along the main axis. Close examination of several similar structures has indicated that this trend was present in the majority of etched NCs. The corrugated morphology of BPO-treated nanorods suggests the anisotropic character of the etching process, which is likely to be the most efficient along impurities and defects of the lattice. Unevenness of etching rates at different sites is also manifested by the highly irregular shape of excessively etched nanorods (Supporting Information Figure SF4), which tend to fragment into smaller segments when the average diameter falls below 2.0−2.2 nm. By using mean dilatation averaging of the lattice fringes in Figure 3a, we identify the position and the approximate size of the CdSe domain in the CdSe/CdS nanorod. The latter was determined to be 3.95 nm, approximately 0.15 nm smaller that the average diameter of the original CdSe seed prior to the growth of CdS extension (see Supporting Information Figure SF3). On the basis of the similarity of the CdS nanorod mean diameter (~4.0 nm) and the size of the incorporated CdSe domain (judging only by the lattice parameter mapping), we conclude that that the layer of CdS material covering the surface of the CdSe dot is likely to be less than one monolayer (0.35 nm).

One of the most basic tests for assessing the effectiveness of the performed etching procedure is obtained through the measurements of changes in the fluorescence (FL) lifetime of CdSe excitations. It is expected that when photoinduced charges are no longer passivated by the potential barrier of the CdS shell, the rate of exciton dissociation due to nonradiative charge transfer to the nanocrystal surface will increase. In this study, we use hole-scavenging mercaptoundecanoic acid (MUA) molecules as ligands on the surface of etched CdSe/CdS dimers in order to facilitate the removal of photoinduced holes. As previous works have shown, the transfer of holes to MUA is very efficient for bare CdSe NCs and results in near-complete quenching of the band gap emission ($\tau_{FL}$ < 0.5 ns).[40] However, in the presence of the CdS shell, the hole transfer rate is reduced due to the potential barrier of the CdS layer, which leads to the enhancement of the emission lifetime and a partial recovery of the NC fluorescence. Consequently, the emission lifetime of MUA-capped NCs is proportional to the thickness of the CdS layers on CdSe[41] and can be used to monitor the extent of CdS etching.


dx.doi.org/10.1021/nl400715n | *Nano Lett.* 2013, 13, 2016−2023

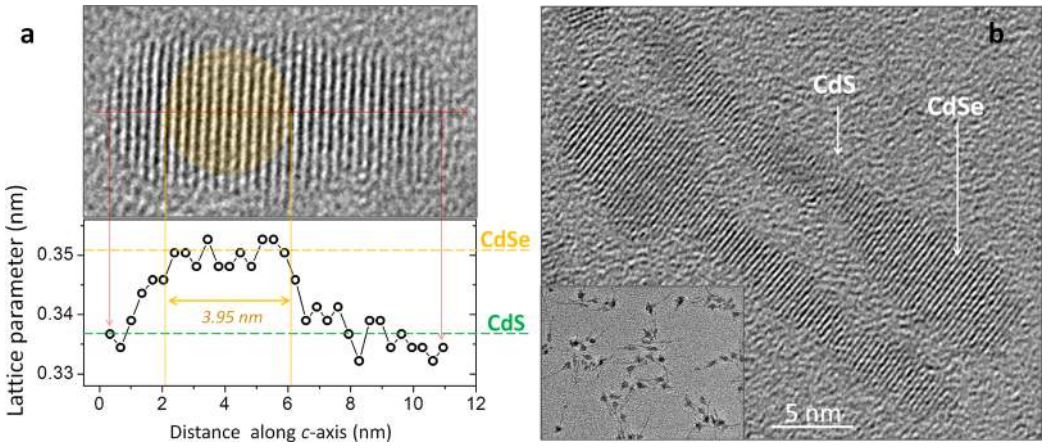


**Figure 3.** (a) A characteristic high-resolution TEM image of an etched CdSe/CdS nanorod. The corresponding lattice spacing along the crystalline *c*-axis of the wurtzite lattice is shown below. The area exhibiting a CdSe lattice parameter is encircled. (b) TEM image of etched CdSe/CdS nanorods comprising large diameter CdSe dots.

Figure 4 illustrates the effect of etching on the fluorescence lifetime of MUA-capped CdSe/CdS nanorods. Prior to BPO treatment, the emission of the CdSe domain decayed in 3.7 ns (Figure 4, red curve), driven primarily by the hole transfer to MUA ligands. Upon removal of approximately 55% of the CdS shell from CdSe/CdS nanostructures (as deduced from the corresponding absorbance change), the FL lifetime of CdSe dots shortened to 1.3 ns. The observed 3-fold decrease in the value of $\tau_{FL}$ confirms an enhanced contribution of photoinduced holes into oxidative reactions on the surface of etched nanocrystals. Indeed, the hole transfer time in MUA-capped CdSe is approximately equal to the FL lifetime of these nanoparticles, when $\tau_{FL}$ is much smaller than the exciton radiative time, $\tau_R$, $\tau_{transfer} = \tau_{FL}/(1 - (\tau_{FL}/\tau_R)) \approx \tau_{FL}$.[42] Therefore, the reduction in the FL lifetime of etched nanocrystals indicates a 3.7/1.3 ≈ 2.85-fold drop in the hole transfer time and an equivalent increase in the rate of oxidative reactions on the surface of the nanoparticle, which may be represented by such processes as ligand or solvent decomposition. Figure 4b confirms a positive correlation of the FL lifetime with the amount of BPO etchant in solution. Expectedly, an enhanced concentration of BPO causes a greater portion of the protective CdS shell to be dissolved, promoting faster tunneling of photoinduced holes from CdSe domains to MUA ligands.

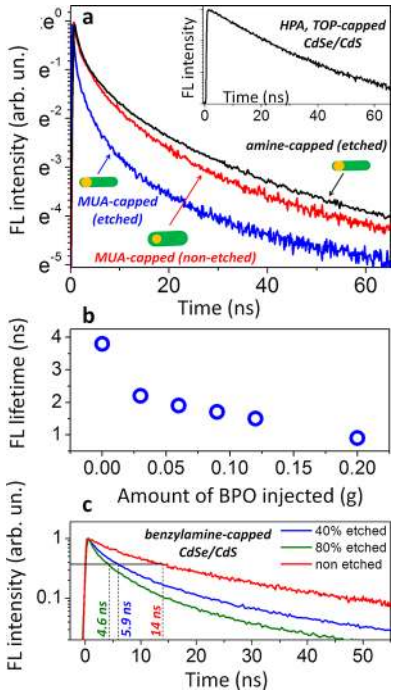


**Figure 4.** (a) Comparison of the fluorescence intensity decay transient for MUA-capped CdSe/CdS nanorods prior (red) and after (blue) etching. Nanocrystals were dissolved in methanol. The insert presents the FL intensity decay of the same nanorods capped with original hydrophobic ligands (HPA, TOP). The FL lifetimes obtained in these measurements were used to calculate the average hole transfer time associated with its transition from CdSe NCs to the surface. The black curve shows the FL intensity decay of benzylamine-capped CdSe/CdS nanorods after etching. (b) The dependence of the fluorescence lifetime of MUA-capped CdSe/CdS nanorods on the extent of etching. The observed trend correlates the decrease in the FL lifetime with the amount of BPO etchant injected into a nanorod solution. (c) The effect of etching on the FL intensity decay of benzylamine-capped CdSe/CdS core/shell nanocrystals. The fraction of etched material refers to the amount of CdS, as estimated from the absorbance profile.

The effect of etching on the rate of charge trapping is investigated in Figure 4c. It is expected that etching-induced defects forming on nanocrystal surfaces will contribute to shortening of the exciton lifetime. If this process constitutes a significant contribution, the reduction in the FL lifetime of etched CdSe/CdS NCs should not be attributed entirely to thinning of the CdS potential barrier between CdSe and MPA, but must partly be ascribed to the enhanced charge trapping on the surface of etched NCs. To investigate this issue we have fabricated spherical core/shell CdSe/CdS NCs and studied the exciton decay dynamics in specimens with partly etched shells. To suppress hole extraction by surface ligands, nonscavenging benzylamine molecules were used on nanoparticle surfaces. According to Figure 4c, continuous removal of the CdS layer in 6.2-nm CdSe/CdS NCs comprising 4.0 nm core (see Supporting Information Figure SF5), results in the gradual drop of the emission lifetime. When most of the shell is etched with less than a monolayer of CdS left on the surface (judging by the intensity of the CdS absorbance feature at $\lambda$ = 450 nm), the FL lifetime drops to 4.6 ns, indicating a potential formation of surface/interfacial defects. Despite charge trapping on defects, the FL lifetime of 80%-etched, benzylamine-passivated


dx.doi.org/10.1021/nl400715n | *Nano Lett.* 2013, 13, 2016−2023

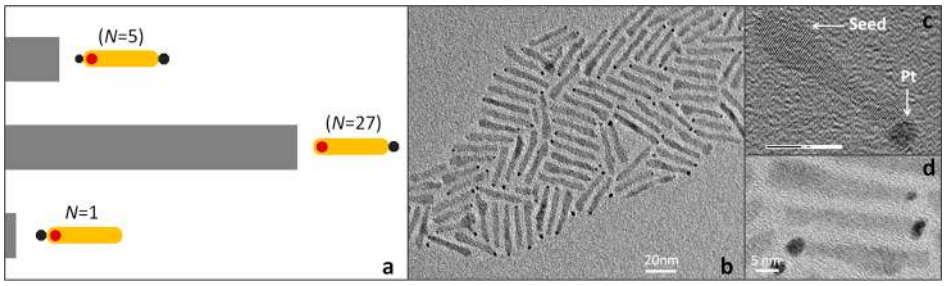


**Figure 5.** TEM analysis of the CdSe/CdS/Pt heteronanocrystals. (a) Statistical distribution of nanoparticle shapes, indicating the preferential growth of the Pt tip opposite from the location of the CdSe seed nanocrystal. (b–d). TEM images of CdSe/CdS/Pt heteronanocrystals. The location of the CdSe seed within CdS nanorods is distinguishable in most structures as a local width enhancement.

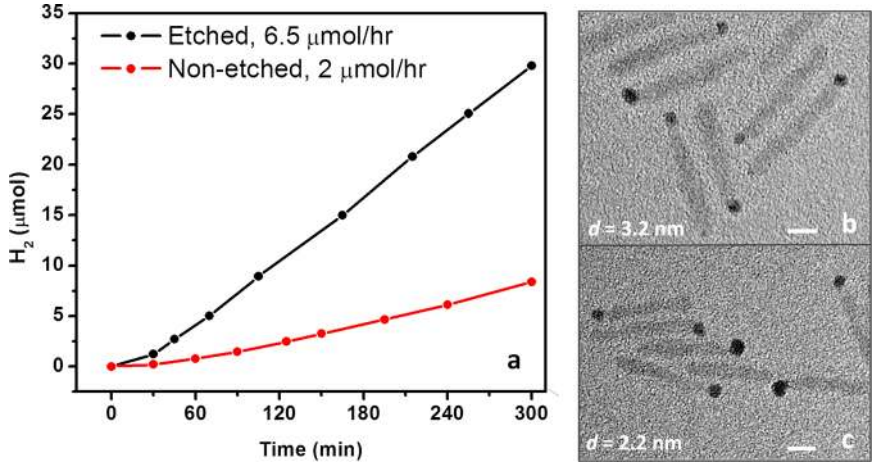


**Figure 6.** (a) Comparison of total amounts of produced $H_2$ between etched (black) and nonetched (red) CdSe/CdS/Pt heteronanocrystals. (b) A TEM image of CdSe/CdS/Pt heteronanocrystals prior to etching. The average diameter is 3.2 nm (scale bar is 5 nm). (c) A TEM image of CdSe/CdS/Pt heteronanocrystals after etching. The average diameter is 2.16 nm (scale bar is 5 nm).

NCs is still 3 times greater than the lifetime of nanocrystals capped with hole-scavenging MUA molecules. Similar trend was observed for benzylamine-passivated CdSe/CdS nanorods, which showed a defect-limited, 5.1 ns FL lifetime upon etching (Figure 4a, black curve). This is 4 times greater than the FL lifetime of the same nanorods strucutres capped with MUA ligands (red curve). On the basis of this difference, we conclude that while etching-induced defects do contribute into exciton decay, this contribution is too small to compete with hole extraction by MUA molecules.

The FL lifetime measurements can also be used to estimate the fraction of the CdS material that was removed during the BPO treatment. The charge transfer rate, $\Gamma_{tunneling}$, is roughly exponential with the shell thickness, $\Delta H_{CdS}$: $\Gamma_{tunneling} \approx 1/\tau_{transfer} \sim \exp(-\Delta H_{CdS})$,[43] such that $1/\tau_{FL} \sim \exp(-\Delta H_{CdS})$. If we assume that etching is spatially isotropic, then the relative reduction in the thickness of the CdS layer covering the surface of CdSe for the sample in Figure 4a can be expressed as: $\exp(-\tau_{FL,\ after})/\exp(-\tau_{FL,\ before}) = \exp(-1.3)/\exp(-3.7) \approx 11$ times. The actual fraction is likely to be lower since the contribution of fast filling trap states into the FL decay is expected to increase upon etching of the CdS surface.

A more rigorous test of the etching effectiveness is provided by the measurements of the CdSe/CdS catalytic activity. To this end, CdSe/CdS nanorods were appended with a Pt catalyst and used for sacrificial generation of hydrogen, as described in ref 33. The dissociation of excitons in the resulting CdSe/CdS/Pt heterostructures is facilitated by the fact that the Pt tip forms primarily on the side of nanorods, which is opposite to the location of the CdSe seed. Such anisotropic growth of Pt was first demonstrated by Mokari et al.[44] and was attributed to the fact that the wurtzite crystalline structure of CdS leads to uneven rates of Pt nucleation on Cd- and S-rich nanorod facets. The statistical analysis of CdSe/CdS/Pt heteronanocrystals fabricated in this work (Figure 5) confirms that more than 80% of nanorods had Pt tips opposite to the location of CdSe seeds. Here, large-diameter CdSe NCs (Supporting Information Figure SF3) were used to "highlight" the location of the seed in the nanorod structure (as illustrated in Figure 5c). In the remaining 20% of structures, a small Pt tip was found near the hole-rich (CdSe) side of the rod in addition to a large-size tip on the opposite end.

It was shown previously that the rate of $H_2$ generation by Pt-tipped CdSe/CdS nanorods is strongly dependent on the rate of hole removal from the positively charged CdSe domain, which affects the probability of backward charge recombination.[33] Under this assumption, etched CdSe/CdS heteronanocrystals should yield a greater $H_2$ production rate since they tend to expel holes at a faster rate. To test this hypothesis, we have fabricated two sets of CdSe/CdS/Pt nanoparticle samples comprising etched and nonetched CdSe/CdS semiconductor nanorods. The etching treatment was applied after the deposition of the Pt tip to ensure that both the size of the CdSe dot and the length of the rod domain remained the same for both samples. TEM images in Figures 6b,c confirm that the size of the Pt catalyst did not decrease significantly due to BPO exposure ($d$(Pt) = 2.62 nm, prior to etching; $d$(Pt) = 2.53 nm, after etching). On the basis of the observed reduction in the


dx.doi.org/10.1021/nl400715n | Nano Lett. 2013, 13, 2016–2023

diameter of CdSe/CdS nanorods from 3.2 nm down to 2.16 nm we estimate that approximately 0.52 nm or 1.5 monolayers of the CdS phase were removed. It should be noted that excessive etching of CdSe/CdS/Pt structures could eventually lead to the decomposition of Pt domains (see Supporting Information Figure SF4), resulting in suppressed $H_2$ production. To ensure that the concentrations of etched and nonetched nanorods during $H_2$ production tests are similar, the optical densities of both nanorod samples at the CdSe absorbance feature ($\lambda$ = 530 nm) were set equal. Since the volume of the CdSe domain does not change significantly during etching (less than 10% as estimated from the exciton peak area), we can expect similar amounts of Pt-tipped structures to be present in both etched and nonetched specimens. Furthermore, since the size of Pt tips was essentially unchanged during etching (less than 4% of difference by size, or 11% by volume), the total amount of Pt in etched and nonetched structures is not expected to differ by more than $(0.10^2 + 0.11^2)^{1/2} \approx 15\%$.

Figure 6 compares $H_2$ production rates, measured on a previously described setup[45] for CdSe/CdS/Pt heteronanocrystals before and after BPO treatment (with concentrations normalized by the CdSe absorbance feature). In both cases, photoinduced holes were regenerated by MUA molecules in $H_2O$ (0.1 M) to eliminate any role of the ligand dissociation on the photocatalytic activity of these materials. For each sample, the optical density and the pH were adjusted to constant values before catalysis. The light source was a 300 W xenon lamp equipped with both a water filter and a 400 nm long pass filter, providing reproducible visible light excitation of each sample. According to Supporting Information Figure SF6, the amount of generated hydrogen scaled linearly with the incident power, indicating that the photon flux was well below the saturation regime. This comes as no surprise since only one photon per 0.5 microsecond is expected to be absorbed by a given nanorod, which is much slower than the hole removal time associated with its transfer to an MUA ligand. Consequently, the observed correlation between enhanced $H_2$ generation and the rate of hole scavenging from the structure is not related to the excitation of secondary electron−hole pairs. Yet, it is well-known that when holes are not removed from the structure efficiently, no hydrogen is produced (for instance, as demonstrated by a recent study in ref 33). The phenomenon was previously ascribed to the possibility of backward recombination between holes and Pt electrons. A recent study[46] has further investigated this issue for the case of Au/CdS heteronanocrystals, concluding that photoinduced holes can be quickly trapped on defect states of the semiconductor/metal interface, which can increase the rate of their backward recombination. Such interfacial trapping is believed to be the primary rate-limiting step in the performed $H_2$ generation experiments on CdSe/CdS/Pt nanorods, which contribution is reduced in etched heterostructures.

Overall, etched CdSe/CdS/Pt nanostructures produced 3−4 times more hydrogen in aqueous media than the original nanorods. This trend was confirmed by several independent tests utilizing different batches of CdSe/CdS/Pt, wherein a typical enhancement of 2.8−3.7 was observed. Consequently, the hydrogen production experiments provide additional evidence suggesting that the exposure of both hole-rich and electron-rich semiconductor domains in complex heteronanocrystals improves their catalytic performance.

The stability of etched samples was comparable to that of original CdSe/CdS/Pt nanorods. On average, a drop in the catalytic hydrogen production rate was observed 48−60 h after the start of the reaction for both etched and nonetched samples. In the long run, benzylamine-passivated nanocrystals were found to be less stable then the ones capped with long-chain ligands showing aggregation after several months in ambient conditions. Batch-to-batch differences in the structure of nanorods (the size of Pt nanoparticle, the quality of Pt/CdS interface, etc.) seemed to have played a greater role in the ultimate stability and efficiency of the catalytic process rather than the degree of nanorods etching. Here, to understand the effect of Pt size on the ensuing hydrogen production rate, two types of CdSe/CdS/Pt structures comprising large ($d$ = 3.1 nm) and small ($d$ = 1.3 nm) Pt tips on identical semiconductor domains were tested. According to Supporting Information Figure SF7, the rate of hydrogen production by optically matched nanorod solutions showed an ∼50% enhancement due to the decrease of Pt tip size.

In conclusion, we demonstrate that chemical etching provides a viable tool for enhancing the catalytic performance of semiconductor heteronanocrystals. This technique complements the traditional approach to nanocrystal synthesis by offering a possibility of fabricating heteronanocrystal morphologies that cannot be easily obtained using colloidal methods. In the present study, a facile etching procedure was employed to fabricate a CdSe/CdS heteronanocrystal dimer where both CdSe and CdS components come into a direct contact with external media. This was achieved by removing an outer layer CdS in dot-in-a-rod CdSe/CdS nanocrystals. Photogenerated hydrogen production tests indicate that catalytic activity of etched materials was enhanced by over 3 times compared to the original CdSe/CdS nanorods. The observed improvement was attributed to the unobstructed transfer of photoinduced holes from the CdSe component to the surface, which rate was increased 3-fold upon etching. We expect that demonstrated application of etching to shaping of colloidal heteronanocrystals can find widespread applications in nanocrystal technologies that require photoinduced charge separation.

## ■ ASSOCIATED CONTENT

### Supporting Information

Details of synthesis. A TEM image of CdSe/CdS nanorods, additional UV−vis spectra, and a TEM image of CdSe/CdS/Pt structures after excessive etching. This material is available free of charge via the Internet at http://pubs.acs.org.

## ■ AUTHOR INFORMATION

### Corresponding Author

*E-mail: zamkovm@bgsu.edu.

### Notes

The authors declare no competing financial interest.

## ■ ACKNOWLEDGMENTS

This work was supported by the NSF under awards CHE-1112227 (M.Z.), CBET-1236355 (M.Z.), and CHE-1012487 (F.C.). We gratefully acknowledge the OBOR "Material Networks" program, Bowling Green State University, and R.S.K. acknowledges support from a McMaster Research Fellowship.

## REFERENCES


(1) Kamat, P. V. Quantum Dot Solar Cells. Semiconductor Nanocrystals as Light Harvesters. *J. Phys. Chem. C* **2008**, *112*, 18737.
(2) Klimov, V. I.; Mikhailovsky, A. A.; Xu, S.; Malko, A.; Hollingsworth, J. A.; Leatherdale, C. A.; Eisler, H.; Bawendi, M. G. Optical gain and stimulated emission in nanocrystal quantum dots. *Science* **2000**, *290*, 314.
(3) Medintz, I. L.; Uyeda, H. T.; Goldman, E. R.; Mattoussi, H. Quantum dot bioconjugates for imaging, labelling and sensing. *Nat. Mater.* **2005**, *4*, 435.
(4) (a) Sun, J.; Zhong, D. K.; Gamelin, D. R. Composite Photoanodes for Photoelectrochemical Solar Water Splitting. *Energy Environ. Sci.* **2010**, *3*, 1252. (b) Riha, S. C.; Fredrick, S. J.; Sambur, J. B.; Liu, Y.; Prieto, A. L.; Parkinson, B. A. Photoelectrochemical Characterization of Nanocrystalline Thin-Film $Cu_2ZnSnS_4$ Photocathodes. *ACS Appl. Mater. Interfaces* **2011**, *3*, 58.
(5) Coe, S.; Woo, W. K.; Bawendi, M.; Bulovic, V. Electroluminescence from single monolayers of nanocrystals in molecular organic devices. *Nature* **2002**, *420*, 800.
(6) Cozzoli, P. D.; Pellegrino, T.; Manna, L. Synthesis, Properties and Perspectives of Hybrid Nanocrystal Structures. *Chem. Soc. Rev.* **2006**, *35*, 1195.
(7) Brown, K. A.; Wilker, M. B.; Boehm, M.; Dukovic, G.; King, P. W. Characterization of Photochemical Processes for $H_2$ Production by CdS Nanorod-[FeFe] Hydrogenase Complexes. *J. Am. Chem. Soc.* **2012**, *134*, 5627.
(8) Mokari, T.; Sztrum, C. G.; Salant, A.; Rabani, E.; Banin, U. Formation of Asymmetric One-Sided Metal Tipped Semiconductor Nanocrystal Dots and Rods. *Nat. Mater.* **2005**, *4*, 855.
(9) Reiss, P.; Protiere, M.; Li, L. Core/Shell Semiconductor Nanocrystats. *Small* **2009**, *5*, 154.
(10) (a) Carbone, L.; Nobile, C.; de Giorgi, M.; Sala, F. D.; Morello, G.; Pompa, P.; Hytch, M.; Snoeck, E.; Fiore, A.; Franchini, I. R.; Nadasan, M.; Silvestre, A. F.; Chiodo, L.; Kudera, S.; Cingolani, R.; Krahne, R.; Manna, L. Synthesis and Micrometer-Scale Assembly of Colloidal CdSe/CdS Nanorods Prepared by a Seeded Growth Approach. *Nano Lett.* **2007**, *7*, 2942. (b) Kumar, S.; Jones, M.; Lo, S. S.; Scholes, G. D. Nanorod heterostructures showing photoinduced charge separation. *Small* **2007**, *3*, 1633.
(11) Shieh, F.; Saunders, A. E.; Korgel, B. A. General Shape Control of Colloidal CdS, CdSe, CdTe Quantum Rods and Quantum Rod Heterostructures. *J. Phys. Chem. B* **2005**, *109*, 8538.
(12) Halpert, J. E.; Porter, V. J.; Zimmer, J. P.; Bawendi, M. G. Synthesis of CdSe/CdTe Nanobarbells. *J. Am. Chem. Soc.* **2006**, *128*, 12590.
(13) Buonsanti, R.; Grillo, V.; Carlino, E.; Giannini, C.; Curri, M. L.; Innocenti, C.; Sangregorio, C.; Achterhold, K.; Parak, F. G.; Agostiano, A.; Cozzoli, P. D. Seeded Growth of Asymmetric Binary Nanocrystals Made of a Semiconductor $TiO_2$ Rodlike Section and a Magnetic $\gamma$-$Fe_2O_3$ Spherical Domain. *J. Am. Chem. Soc.* **2006**, *128*, 16953.
(14) Acharya, K. P.; Alabi, T. R.; Schmall, N.; Hewa-Kasakarage, N. N.; Kirsanova, M.; Nemchinov, A.; Khon, E.; Zamkov, M. Linker-Free Modification of $TiO_2$ Nanorods with PbSe Nanocrystals. *J. Phys. Chem. C* **2009**, *113*, 19531.
(15) Acharya, K. P.; Hewa-Kasakarage, N. N.; Alabi, T. R.; Nemitz, I.; Khon, E.; Ullrich, B.; Anzenbacher, P.; Zamkov, M. Synthesis of PbS/$TiO_2$ Colloidal Heterostructures for Photovoltaic Applications. *J. Phys. Chem. C* **2010**, *114*, 12496.
(16) Bao, Z. H.; Sun, Z. H.; Xiao, M. D.; Chen, H. J.; Tian, L. W.; Wang, J. F. Transverse Oxidation of Gold Nanorods Assisted by Selective End Capping of Silver Oxide. *J. Mater. Chem.* **2011**, *21*, 11537.
(17) Tsung, C. K.; Kou, X.; Shi, Q.; Zhang, J.; Yeung, M. H.; Wang, J.; Stucky, G. D. Selective Shortening of Single-Crystalline Gold Nanorods by Mild Oxidation. *J. Am. Chem. Soc.* **2006**, *128*, 5352.
(18) Sreeprasad, T. S.; Samal, A. K.; Pradeep, T. Body- or Tip-Controlled Reactivity of Gold Nanorods and Their Conversion to Particles through Other Anisotropic Structures. *Langmuir* **2007**, *23*, 9463.
(19) Zou, R. X.; Guo, X.; Yang, J.; Li, D. D.; Peng, F.; Zhang, L.; Wang, H. J.; Yu, H. Selective Etching of Gold Nanorods by Ferric Chloride at Room Temperature. *CrystEngComm* **2009**, *11*, 2797.
(20) Guo, X.; Zhang, Q.; Sun, Y.; Zhao, Q.; Yang, J. Lateral Etching of Core-Shell Au@Metal Nanorods to Metal-Tipped Au Nanorods with Improved Catalytic Activity. *ACS Nano* **2012**, *6*, 1165.
(21) Matsumoto, H.; Sakata, T.; Mori, H.; Yoneyama, H. Preparation of Monodisperse CdS Nanocrystals by Size Selective Photocorrosion. *J. Phys. Chem.* **1996**, *100*, 13781.
(22) Torimoto, T.; Hashitani, M.; Konishi, T.; Okazaki, K.; Shibayama, T.; Ohtani, B. Photochemical Shape Control of Cadmium Sulfide Nanorods Coated with an Amorphous Silica Thin Layer. *J. Nanosci. Nanotechnol.* **2009**, *9*, 506.
(23) Liu, J.; Aruguete, D. M.; Jinschek, J.; Rimstidt, J. D.; Hochella, M. F., Jr. The Non-Oxidative Dissolution of Galena Nanocrystals: Insights into Mineral Dissolution Rates as a Function of Grain Size, Shape and Aggregation State. *Geochim. Cosmochim. Acta* **2008**, *72*, 5984.
(24) Liu, L.; Peng, Q.; Li, Y. Preparation of CdSe Quantum Dots with Full Color Emission Based on a Room Temperature Injection Technique. *Inorg. Chem.* **2008**, *47*, 5022.
(25) Torimoto, T.; Murakami, S.; Sakuraoka, M.; Iwasaki, K.; Okazaki, K.; Shibayama, T.; Ohtani, B. Photochemical Fine-Tuning of Luminescent Color of Cadmium Selenide Nanoparticles: Fabricating a Single-Source Multicolor Luminophore. *J. Phys. Chem. B* **2006**, *110*, 13314.
(26) Galian, R. E.; de la Guardia, M.; Pérez-Prieto, J. Photochemical Size Reduction of CdSe and CdSe/ZnS Semiconductor Nanoparticles Assisted by $n\pi^*$ Aromatic Ketones. *J. Am. Chem. Soc.* **2009**, *131*, 892.
(27) Liu, J.; Yang, X.; Wang, K.; Wang, D.; Zhang, P. Chemical etching with tetrafluoroborate: a facile method for resizing of CdTe nanocrystals under mild conditions. *Chem. Commun.* **2009**, *2009*, 6080.
(28) Uematsu, T.; Kitajima, H.; Kohma, T.; Torimoto, T.; Tachibana, Y.; Kuwabata, S. Tuning of the fluorescence wavelength of CdTe quantum dots with 2 nm resolution by size-selective photoetching. *Nanotechnology* **2009**, *20*, 215302.
(29) Talapin, D. V.; Gaponik, N.; Borchert, H.; Rogach, A. L.; Haase, M.; Weller, H. Etching of Colloidal InP Nanocrystals with Fluorides: Photochemical Nature of the Process Resulting in High Photoluminescence Efficiency. *J. Phys. Chem. B* **2002**, *106*, 12659.
(30) Lim, S. J.; Kim, W.; Jung, S.; Seo, J.; Shin, K. S. Anisotropic Etching of Semiconductor Nanocrystals. *Chem. Mater.* **2011**, *23*, 5029.
(31) (a) She, C. X.; Demortière, A.; Schevchenko, E. V.; Pelton, M. Using Shape To Control Photoluminescence From Cdse/Cds Core/Shell Nanorods. *J. Phys. Chem. Lett.* **2011**, *2*, 1469. (b) Scholes, G. D.; Jones, M.; Kumar, S. Energetics of Photoinduced Electron-Transfer Reactions Decided by Quantum Confinement. *J. Phys. Chem. C* **2007**, *111*, 13777.
(32) Amirav, L.; Alivisatos, P. A. Photocatalytic Hydrogen Production with Tunable Nanorod Heterostructures. *J. Phys. Chem. Lett.* **2010**, *1*, 1051.
(33) Acharya, K. P.; Khnayzer, R. S.; O'Connor, T.; Diederich, G.; Kirsanova, M.; Klinkova, A.; Roth, D.; Kinder, E.; Imboden, M.; Zamkov, M. The Role of Hole Localization in Sacrificial Hydrogen Production by Semiconductor−Metal Heterostructured Nanocrystals. *Nano Lett.* **2011**, *11*, 2919.
(34) Bao, N.; Shen, L.; Takata, T.; Domen, K. Self-Templated Synthesis of Nanoporous CdS Nanostructures for Highly Efficient Photocatalytic Hydrogen Production under Visible Light. *Chem. Mater.* **2008**, *20*, 110.
(35) Elmalem, E.; Saunders, A. E.; Costi, R.; Salant, A.; Banin, U. Growth of Photocatalytic CdSe−Pt Nanorods and Nanonets. *Adv. Mater.* **2008**, *20*, 4312.
(36) Berr, M.; Vaneski, A.; Susha, A. S.; Rodríguez-Fernández, J.; Döblinger, M.; Jäckel, F.; Rogach, A. L.; Feldmann, J. Colloidal CdS nanorods Decorated with Subnanometer Sized Pt Clusters for Photocatalytic Hydrogen Generation. *J. Appl. Phys. Lett.* **2010**, *97*, 093108.

(37) Zhu, H.; Song, N.; Lv, H.; Hill, C. L.; Lian, T. Near Unity Quantum Yield of Light-Driven Redox Mediator Reduction and Efficient $H_2$ Generation Using Colloidal Nanorod Heterostructures. *J. Am. Chem. Soc.* **2012**, *134*, 11701.
(38) Yu, W. W.; Qu, L.; Guo, W.; Peng, X. Experimental determination of the extinction coefficient of CdTe, CdSe, and CdS nanocrystals. *Chem. Mater.* **2003**, *15*, 2854.
(39) Battaglia, D.; Blackman, B.; Peng, X. G. Coupled and Decoupled Dual Quantum Systems in One Semiconductor Nanocrystal. *J. Am. Chem. Soc.* **2005**, *127*, 10889.
(40) Völker, J.; Zhou, X. Y.; Ma, X.; Flessau, S.; Lin, H. W.; Schmittel, M.; Mews, A. Semiconductor Nanocrystals with Adjustable Hole Acceptors: Tuning the Fluorescence Intensity by Metal−Ion Binding. *Angew. Chem., Int. Ed.* **2010**, *49*, 6865.
(41) O'Connor, T.; Panov, M.; Mereshchenko, A.; Tarnovsky, A. N.; Lorek, R.; Perera, D.; Diederich, G.; Lambright, S.; Moroz, P.; Zamkov, M. The Effect of the Charge-Separating Interface on Exciton Dynamics in Photocatalytic Colloidal Heteronanocrystals. *ACS Nano* **2012**, *6*, 8156.
(42) Perera, D.; Lorek, R.; Khnayzer, R. S.; Moroz, P.; O'Connor, T.; Khon, D.; Diederich, G.; Kinder, E.; Lambright, S.; Castellano, F. N.; Zamkov, M. Photocatalytic Activity of Core/Shell Semiconductor Nanocrystals Featuring Spatial Separation of Charges. *J. Phys. Chem. C* **2012**, *116*, 22786.
(43) Khon, E.; Lambright, S.; Khon, D.; Smith, B.; O'Connor, T.; Moroz, P.; Imboden, M.; Diederich, G.; Perez-Bolivar, D.; Anzenbacher, P.; Zamkov, M. Inorganic Solids of CdSe Nanocrystals Exhibiting High Emission Quantum Yield. *Adv. Funct. Mater.* **2012**, *22*, 3714.
(44) Habas, S. E.; Yang, P.; Mokari, T. Selective Growth of Metal and Binary Metal Tips on CdS Nanorods. *J. Am. Chem. Soc.* **2008**, *130*, 3294−3295.
(45) Wang, X.; Goeb, S.; Ji, Z.; Pogulaichenko, N. A.; Castellano, F. N. Homogeneous Photocatalytic Hydrogen Production Using $\pi$-Conjugated Platinum(II) Arylacetylide Sensitizers. *Inorg. Chem.* **2011**, *50*, 705.
(46) Khon, E.; Mereshchenko, A.; Tarnovsky, A.; Acharya, K.; Klinkova, A.; Hewa-Kasakarage, N.; Nemitz, I.; Zamkov, M. Suppression of the Plasmon Resonance in Au/CdS Colloidal Nanocomposites. *Nano Lett.* **2011**, *11*, 1792−1799.